Journal of Alloys and Compounds, 207/208 (1994) 372–376
JALCOM 3061

Crystal structure and hydriding behavior of $LaNi_{5-y}Sn_y$

J.S. Cantrell and T.A. Beiter
Chemistry Department, Miami University, Oxford, OH 45056 (USA)

R.C. Bowman, Jr.*
Aerojet Electronic Systems Division, Azusa, CA 91702 (USA)

Abstract

The phase composition and structures of several $LaNi_{5-y}Sn_y$ alloys with $y<0.3$ have been studied using X-ray diffraction. These alloys are found to retain the hexagonal symmetry of $LaNi_5$ with increases in both lattice parameters. Since the Sn atoms are larger than the Ni atoms which are being replaced, small distortions are likely to arise in the positions of the Ni atoms located at the midplane 3g sites that are above and below the Sn atoms. Effects of variations in alloy stoichiometry and hydrogen absorption/desorption under different conditions are also reported.

1. Introduction

It is widely known that the hexagonal intermetallic compound $LaNi_5$ possesses exceptional hydriding properties. With little or no activation treatment, $LaNi_5$ can absorb more than six hydrogen atoms per formula unit across a nearly flat plateau pressure of 2 atm at room temperature. Furthermore, the absorption–desorption hysteresis ratio is modest and the kinetics are extremely fast. Another attractive attribute of $LaNi_5$ is the large modifications in hydriding behavior that are produced by elemental substitution for La and Ni [1–3]. These combinations of properties for the substituted $LaNi_5$ alloys have led to numerous proposals for their utilization in hydrogen storage and energy conversion applications [4]. However, the hydrides of $LaNi_5$ and most of its substituted alloys have been found [5–7] to degrade rather severely (*i.e.* losses in reversible hydrogen storage capacities up to 60–80% of its initial values and large variations in the absorption desorption isotherms) during thermal cycling and aging at temperatures above 450 K. This lack of stability seriously impedes the performance of these hydrides in devices that must produce high pressures over 10^3–10^5 absorption–desorption cycles.

The substitution of Al in $LaNi_{5-y}Al_y$ alloys with $y<1.0$ does reduce the degree of degradation [8,9]. However, Al-substitution also reduces hydrogen storage capacity, decreases the plateau pressure, and slows the hydrogen diffusion rate.

Lambert *et al.* [7] recently reported that tin substitutions for nickel of $y\approx0.2$ substantially reduced the intrinsic degradation of the $LaNi_{4.8}Sn_{0.2}H_x$ phase during thermal cycling and aging without a major decrease in storage capacity. Although the plateau pressures were lower for $LaNi_{4.8}Sn_{0.2}H_x$ compared to $LaNi_5H_x$, Sn substitution also led to a significant decrease in the hysteresis ratio [3,7], which is highly desirable in many applications. Furthermore, the lattice strain derived [7] from linewidths of the X-ray diffraction peaks was significantly smaller for the $LaNi_{4.8}Sn_{0.2}$ alloy after hydriding when compared to $LaNi_5$ or $La_{0.9}Gd_{0.1}Ni_5$. In order to gain a better understanding of the reasons for these changes with Sn substitution, further studies were made of the hydriding behavior and the structural properties of $LaNi_{5-y}Sn_y$. The present paper primarily addresses the results obtained by powder X-ray diffraction measurements and analyses.

2. Alloy preparation and hydriding behavior

Percheron and Welter [10] have discussed how various factors associated with the production and handling of hydrogen storage alloys can strongly impact subsequent hydriding reactions and so-called equilibrium properties. In fact, the metal hydride literature abounds with apparently contradictory observations on the behavior

*Author to whom correspondence should be addressed.

SSDI 0925-8388(93)03061-M

of specific substitutional elements in the AB_5 alloy system. Gschneidner [11] has recently emphasized that chemical impurities in rare earth metals can stabilize alternative phases in alloys as well as modify critical physical properties.

Recognizing the potential importance of variations in alloy stoichiometry and La metal purity on the hydriding behavior of nominal $LaNi_{4.8}Sn_{0.2}$, a variety of samples were examined. With the exception of the La-rich alloy $LaNi_{4.41}Sn_{0.245}$ provided by Hydrogen Consultants, Inc. and used in a past hydride compressor test study [12], all other alloys were prepared at the Ames Laboratory of Iowa State University. Smaller samples containing high purity (HP) La metal (*i.e.* purity > 99.95 at.%) were prepared by arc-melting while larger (*i.e.* several kg) batches using 99+% La were formed by vacuum induction and casting. All $LaNi_{5-y}Sn_y$ alloys were vacuum annealed at nominal 1225 K for 3–5 days. Optical metallography confirmed that all the Ames Laboratory samples were single phase after the annealing. Chemical analyses of metal compositions and total oxygen contents were also done at Ames Laboratory.

Representative room temperature (*i.e.* 298 K) hydrogen absorption–desorption isotherms for three $LaNi_{5-y}Sn_y$ alloys are compared in Fig. 1. The pressure is shown on a linear scale (rather than conventional $\ln P$) to emphasize the slopes across the plateau and the hysteresis. The isotherms for the $LaNi_{4.41}Sn_{0.245}$ alloy are taken from ref. 12 and have no data below $x = 1.0$ as the pressures were quite low at these compositions. While the maximum hydrogen content is $x = 6$ for the three alloys, several differences are apparent in Fig. 1. First, the plateau begins near $x = 0.5$ for the two nominal $LaNi_{4.8}Sn_{0.2}$ alloys while it does not begin until nearly $x = 1.5$ for the non-stoichiometric $LaNi_{4.41}Sn_{0.245}$ alloy. It should be noted that the hydrogen corresponding to this region can be reversibly removed by evacuation and does not appear to correspond to a secondary phase. The slopes for the absorption and desorption plateaus are smallest for the high purity alloy while the hysteresis ratios are equivalent within the data uncertainties.

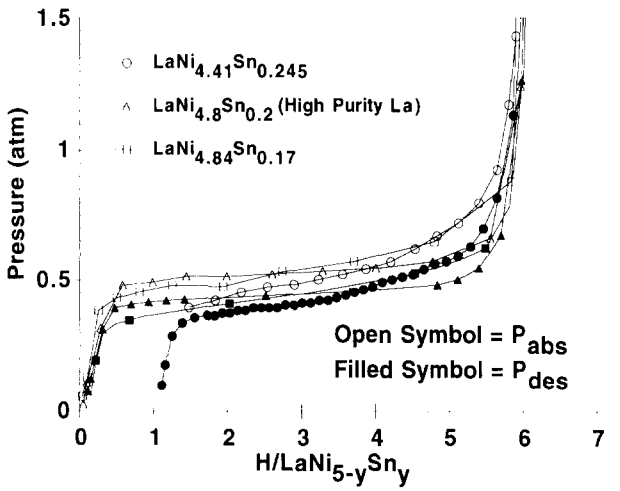

Fig. 1. Hydrogen absorption (P_{abs}) and desorption (P_{des}) isotherms at 298 K for three $LaNi_{5-y}Sn_y$ alloys.

3. X-Ray diffraction results and interpretation

The powder $LaNi_{5-y}Sn_y$ samples were examined as previously described [13]. Flat samples were placed on a microscope slide using an adhesive for automated step scans on a Rigaku horizontal, wide angle, automated diffractometer operating at 40 kV and 40 mA for a copper anode. The data were recorded at 0.05° 2θ steps with a 2-s count time. A nickel filter was used to reduce Cu Kβ radiation. A reference standard of silicon 640a (National Institute of Science and Technology) was used and the X-ray diffraction (XRD) pattern analysis was conducted using programs by Goehner [14], Jendrek [15], Smith *et al.* [16] and Beiter [17].

The X-ray diffraction patterns obtained from the $LaNi_{5-y}Sn_y$ alloys indicate a hexagonal structure that is closely related to that shown in Fig. 2 for stoichiometric $LaNi_{5.0}$, which belongs to the space group *P6/mmm*. The lattice parameters and unit cell volumes for several $LaNi_{5-y}Sn_y$ alloys are summarized in Table 1 along with other crystallographic properties. As reported previously [2,7], Sn substitution increases the lattice parameters and cell volumes. Variations in stoichiometry and oxygen impurity levels also affect the lattice properties, but no systematic trend is apparent in Table 1. The methods of preparation can influence composition homogeneity and strain disorder. Furthermore, the nominal $LaNi_5$ phase can accommodate an excess of 3d metals *via* randomly distributed structural defects where

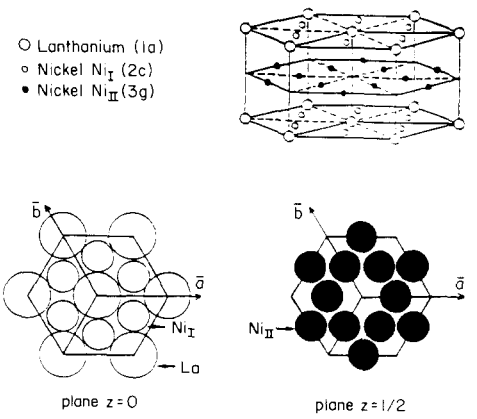

Fig. 2. Positions of metal atoms in the hexagonal $LaNi_5$ structure with space group type *P6/mmm*.

TABLE 1. Lattice parameters and other properties of $LaNi_{5-y}Sn_y$

Alloy composition	High purity La used	Oxygen content[b] (at.%)	a (nm)	c (nm)	c/a	Cell volume (10^{-2} nm^3)
$LaNi_{4.98}Sn_{0.20}$[a]	No	0.08	0.5049(1)	0.4021(1)	0.7964	8.878(4)
$LaNi_{4.95}Sn_{0.095}$[a]	Yes	0.04	0.5034(1)	0.3997(1)	0.7939	8.772(2)
$LaNi_{4.84}Sn_{0.20}$[a]	Yes	0.06	0.5060(1)	0.4022(1)	0.7949	8.921(2)
$LaNi_{4.84}Sn_{0.17}$[a]	No	0.15	0.5057(1)	0.4014(3)	0.7938	8.891(6)
$LaNi_{4.80}Sn_{0.20}$	Yes	–	0.5031(2)	0.4028(2)	0.8006	8.907(5)
$LaNi_{5.00}$	Yes	0.05	0.5024(1)	0.3978(1)	0.7919	8.695(10)
$LaNi_{4.41}Sn_{0.245}$[a]	No	0.89	0.5060(2)	0.4021(2)	0.7947	8.916(6)

[a]Determined by elemental analysis using inductively-coupled-plasma atomic emission spectroscopy.
[b]Determined by the inert gas fusion method using a LECO instrument.

the La atoms in the la position of the *P6/mmm* space group are replaced by pairs of Ni (or other 3d) atoms that are aligned along the sixfold *c*-axis [19,20]. The volume increases very rapidly with Sn substitution in comparison with most other elements for Ni [2,3]. This is not surprising since Sn is much larger than Ni. Percheron *et al.* [3,18] have described the distribution of several substitutional atoms in $La_xNi_{5-y}M_y$ where M is Al, Si, Fe, Mn, or Cu. They observed that most often Ni atom replacement occurs mainly at the 3g-site in the $z=1/2$ plane (see Fig. 2 for clarification) except for Cu which has a slight preference for the 2c-sites in the $z=0$ planes. While these atoms are 2.2–15% larger than Ni, the Sn atom is over 30% larger. Consequently, it is highly unlikely that the Sn atoms can occupy either 2c or 3g sites without severe distortions and/or displacements of neighboring La and Ni atoms. The non-La metals (Ni+Sn) to La ratio varies (Table 1) from 4.66 to 5.20 but these composition changes are not correlated to the *c/a* values or unit cell volumes. This implies the presence of a defect phase or a non-stoichiometric phase which has Sn substituted for Ni randomly but approximately in every fourth unit cell. There may also be some interstitial substitution but the narrow XRD lines indicate good crystallographic material.

The X-ray diffraction patterns indicated that all of the alloys are hexagonal and isomorphous. The only space group that would solve the powder X-ray diffraction intensity patterns is *P6/mmm* (191) with shear and stacking fault disorder (given in Table 2) and with atomic positions *a* (0,0,0), *c* (1/3,2/3,0) and (2/3,1/3,0) and *g* (1/2,0,1/2), (0,1/2,1/2) and (1/2,1/2,1/2). The structure of the substituted alloys is essentially the same as the parent material, $LaNi_5$. Other hexagonal space group's atomic position refinement did not solve the data sets. The shear and stacking fault displacements and population fractions (Table 2) were refined along with isotropic temperature terms and occupancy coefficients for the c and g sites. Since the powder diffraction intensities are relative and not absolute intensities, only relative occupancy coefficients can be obtained from the refinement, *i.e.* one of the occupancy coefficients must be fixed throughout the refinement to a prechosen value. The fixed occupancy was chosen to be the lanthanum at (0,0,0) with unit coefficient on the lanthanum atomic scattering function.

The occupancy coefficients have been refined to indicate the tin sites, the larger occupancy values indicating the presence of tin atoms on a statistical distribution basis but without long range ordering since no super lattice diffraction peaks could be found. The history of the individual samples appears to affect the amount and type of disorder but not the phase of the alloy. Rapid quenching, annealing and hydrogen absorption/desorption cycling also affect the disorder parameters but do not change the phase for these alloys. The starting alloy shows very little XRD evidence for other phases even when some oxgyen was found by chemical analyses, however EDAX (energy dispersive analysis by X-rays) and metallography studies on a couple of samples did show minor amounts of other phases at grain boundaries. Most of the oxygen appears to be present on the surfaces of the powder particles as binary oxides or hydroxides of La but these layers are not thick enough to give XRD lines unless the sample is heated in air for some time. No oxide phases could be identified in the XRD patterns in the data for the samples reported in Tables 1 and 2.

The *R* factors range from 0.033 to 0.065 for the data sets in Table 2 which also lists the occupancy factors for the La, Ni(2c) and Ni(3g) sites for the small range of metal atom compositions given in Table 1. When occupancy factors exceed 1.0 for Ni, Sn substitution is indicated (due to larger *Z*). Note that the occupancy factors may not sum to the analytical Sn+Ni values due to the disorder. Sn substitution for Ni results in disorder due to the larger size of Sn. This disorder is due to the incorporation of Sn atoms that occupy a place near the crystallographic c-sites, usually in every fourth unit cell (c1 and c2 sites are apparently disordered in Sn occupancy). The c-sites in the $z=0$ plane (Fig.

TABLE 2. Structural parameters for the intermetallic compounds $LaNi_{5-y}Sn_y$

Alloy composition	R factor	Atomic populations[a]			Sn+Ni[b]	Temperature factors			Principal disorder vector(s)[c]	No. of intensity data
		La	Ni(c)	Ni(g)		La	Ni(c)	Ni(g)		
$LaNi_{4.98}Sn_{0.20}$	0.062	1.00	0.97	1.13	5.18	2.8	3.1	4.8	S+SF PFO [211]	126
$LaNi_{4.95}Sn_{0.095}$	0.054	1.00	1.02	0.95	5.045	3.4	4.3	3.6	SF	138
$LaNi_{4.84}Sn_{0.20}$	0.033	1.00	1.02	1.02	5.04	2.3	4.2	3.1	S+SF	141
$LaNi_{4.84}Sn_{0.17}$	0.065	1.00	0.94	0.88	5.01	2.8	2.4	1.9	S+SF PFO [112]	135
$LaNi_{4.80}Sn_{0.20}$	0.069	1.00	0.88	0.86	5.00	1.4	1.6	1.9	S+SF	141
$LaNi_{5.00}$	0.051	1.00	1.04	1.00	5.00	1.2	0.8	0.5	SF	138
$LaNi_{4.41}Sn_{0.245}$	0.050	1.00	0.98	0.96	4.655	3.3	2.0	1.7	S+SF PFO [211]	108

[a]Atomic population are fit to the powder XRD intensity data, La is set to 1.0. These coefficients may not sum to the analytical value (Sn+Ni) because of the disorder that is present.
[b]Determined by elemental analysis using inductively coupled plasma atomic emission spectroscopy.
[c]S, shear; SF, stacking fault; PFO, preferred orientation [*hkl*].

2) are near the La atom at the origin (1a-site). Considerable improvement is achieved in lowering the *R* factors when structural disorder (usually shear) or stacking faults are included in the refinement. In Table 2, the Ni temperature factors (*B*) are larger for the Ni+Sn rich alloys and both the c- and g-sites show Sn substitution (based on occupancy coefficients (in Table 2), while the lower Ni+Sn ratio alloys show less Sn substitution especially in the g-sites but show a small preference for the c-sites. They also have lower temperature factors *B*(Ni(c)) and *B*(Ni(g)) indicating the Ni+Sn rich alloys to be more disordered. It is possible that when neighboring unit cells are considered, the Ni in layers above and below the Sn will be found to shift slightly which may have a stabilizing effect on this structure by an intermetallic coordination, holding the structure together for an accordion-type motion during hydriding and dehydriding as the unit cell expands and contracts. This may be one of the structural features that leads to the greater resistance to intrinsic degradation of the $LaNi_{4.8}Sn_{0.2}H_x$ phase when compared to $LaNi_5H_x$ as described previously by Lambert *et al.* [7]. It is proposed by these studies that some form of shear, stacking fault disorder or micro-twinning is occurring in the $LaNi_{5-y}Sn_y$ alloys where the Sn atoms are disordered but primarily in c-sites. Further studies will be required to resolve these issues.

Acknowledgments

We thank B. Beaudry and T. Ellis for preparation of the alloys, Professor T.B. Flanagan and his colleagues for measurements of the isotherms of several alloys and E. Jendrek for computer and diffractometer support.

References

1 H.H. van Mal, K.H.J. Buschow and A.R. Miedema, *J. Less-Common Met., 35* (1974) 65.
2 M. Mendelsohn, D. Gruen and A. Dwight, *Inorg. Chem., 18* (1979) 3343.
3 A. Percheron-Guegan, C. Lartigue and J.C. Achard, *J. Less-Common Met., 109* (1985) 287.
4 G. Sandrock, S. Suda and L. Schlapbach, in L. Schlapbach (ed.), *Hydrogen in Intermetallic Compounds II*, Springer-Verlag, Berlin, 1992, p. 197.
5 G.D. Sandrock, *Z. Phys. Chem. N.F., 164* (1989) 225.
6 H.-J. Ahn and J.-Y. Lee, *Int. J. Hydrogen Energy, 16* (1991) 93.
7 S.W. Lambert, D. Chandra, W.N. Cathey, F.E. Lynch and R.C. Bowman, Jr., *J. Alloys Comp., 187* (1992) 113.
8 J.M. Park and J.-Y. Lee, *Mater. Res. Bull., 22* (1987) 455.
9 P.D. Goodell, *J. Less-Common Met., 99* (1984) 1.
10 A. Percheron-Guegan and J.-M. Welter, in L. Schlapbach (ed.), *Hydrogen in Intermetallic Compounds I*, Springer-Verlag, Berlin, 1988, p. 11.
11 K.A. Gschneidner, Jr., *J. Alloys Comp., 193* (1993) 1.
12 R.C. Bowman, Jr., B.D. Freeman, D. Labor, F.E. Lynch, R.W. Marmaro and L.A. Wade, *Proc. 7th Int. Cryocooler Conf.*, Santa Fe, NM, 1992, USAF Phillips Laboratory Report PL-CP-93-1001, pp. 867–879.
13 R.C. Bowman, Jr., J.S. Cantrell, A.J. Maeland, A. Attalla and G.C. Abell, *J. Alloys Comp., 185* (1992) 7.
14 R.P. Goehner, in J.R. Rhodes, C.S. Barrett, D.E. Leyden, J.B. Newkirk, P.K. Predecki and C.O. Ruud (eds.), *Advances in X-Ray Analysis*, Plenum, New York, 1980, Vol. 23, pp. 305–311.

15 E.F. Jendrek, Modification of program LATTICE by D.E. Appleman and H.T. Evans, USGSI-GD-73-003, US Geological Survey Report, Washington, DC, 1973.
16 D.K. Smith, M.C. Nichols and M.E. Zolinsky, *POWD, A FORTRAN IV Program for Calculating X-ray Diffraction Patterns-Version 10*, Pennsylvania State University, University Park, PA, 1983.
17 T.A. Beiter, A new structure determining algorithm using powder or single crystal x-ray diffraction intensities and several related results, *Dissertation,* Miami University, Chemistry Department, Oxford, OH 45056, 1992.
18 A. Percheron-Guegan, C. Lartigue and J.C. Achard, *J. Less-Common Met., 74* (1980) 1.
19 K.H.J. Buschow and H.H. van Mal, *J. Less-Common Met., 29* (1972) 203.
20 W. Coene, D.H.L. Notten, F. Hakkens, R.E.F. Einerhand and J.L.C. Daams, *Philos. Mag., A65* (1992) 1485.